Feasibility Study of Quasi-Optical MIMO Antennas for Radiative Near-Field Links

Llombart, Nuria; Dabironezare, Shahab Oddin

DOI
10.1109/TAP.2022.3168724

Publication date
2022

Document Version
Final published version

Published in
IEEE Transactions on Antennas and Propagation

Feasibility Study of Quasi-Optical MIMO Antennas for Radiative Near-Field Links

Nuria Llombart, *Fellow, IEEE*, and Shahab Oddin Dabironezare, *Member, IEEE*

***Abstract*— This article presents a feasibility study of single feed per beam quasi-optical (QO) antennas for enabling incoherent multiple-input multiple-output (MIMO) array front-end architectures at 270 GHz. The objective is to reach ultrafast and radiated energy efficient point-to-point (PtP) wireless links by exploiting the multimode capacity of radiative (Fresnel region) near-field links. In this article, we present a feasibility study of the number of independent links achievable with QO MIMO incoherent arrays. For this purpose, we present theoretical curves of the level of EM co-coupling and interference between the multiple modes versus the link distance. The study focuses at the 252–325 GHz spectral bandwidth defined by the new IEEE 802.15.3d standard. A specific and new MIMO array architecture operating at 270 GHz based on a 2 × 2 array of parabolic reflectors is proposed for a link distance of 100 m. The proposed PtP MIMO system is capable of generating 16 dual-polarized modes in a 70 GHz bandwidth with signal-to-interference ratio >17 dB and a power co-coupling coefficient of −3 dB without the need for interference cancelation techniques. Combining this architecture with wideband front ends could potentially lead to an aggregated data rate in the order of terabit per second in a PtP wireless line-of-sight link, not previously achieved experimentally to the best of authors' knowledge.**

***Index Terms*— Multiple-input multiple-output (MIMO), quasi-optical (QO) antennas, sub-THz, wireless links.**

I. Introduction

As DATA traffic in cellular networks keeps increasing, extremely high backhauling speeds will be needed in future 6G applications with radiated energy efficient system architectures [1]. Current microwave wireless links follow the classical far-field Friis equation, excluding fading and multipath effects, where the transmitted electromagnetic energy presents a spherical spatial spreading. This spreading leads to orders of magnitude lower received power than the one transmitted, and therefore to low radiated energy efficiency [2]. On top of that, in order to reach a high bit/s rate with a small radio frequency (RF) bandwidth with low detection errors, the detected signal has to be orders of magnitude above the thermal noise. Therefore, current wireless links rely heavily on electronic amplification, which requires significant extra dc energy [3]. The use of millimeter wavelengths with larger available bandwidth has already been proposed in 5G networks as an alternative solution [4]. One step further can be reached with the exploitation of higher frequencies carriers (>100 GHz) [1]. For instance, the new IEEE 802.15.3d standard [5] considers up to 70 GHz in the H-band (252–325 GHz). However, there are important challenges for exploiting this spectral bandwidth due to the limited performance of integrated technology (low RF power, nonlinearities, and high electronic noise) [6]. Therefore, new communication system architectures based on low RF power levels and basic signal processing techniques are needed for the practical exploitation of this frequency band.

At microwave frequencies, the spectral capacity for a certain bandwidth is improved via massive multiple-input multiple-output (MIMO) architectures [7], [8], exploding the rich scattering in the non-line-of-sight (NLoS) fading channels. When moving to mm-wave frequency and outdoor ranges, with limited scattering in the propagation environment, the use of line-of-sight (LoS) MIMO for point-to-point (PtP) links has been proposed instead [9]–[13], where directive antenna arrays are properly distributed to increase the channel capacity via relative phase shifts and summations of the received signals or using precoding techniques. In the optical domain, the concept of exploiting orbital angular momentum (OAM) in the phase distribution of an electromagnetic field has also been proposed to increase the number of PtP links [14], [15]. At millimeter frequencies, antenna arrays have also been proposed to generate such phase modes [16], [17], leading to about 3–6 independent spatial data streams. However, it has been argued that there is no real advantage of such approach with respect to a more classical MIMO implementation [18]. At far-field distances, only the main OAM mode remains, and in near-field distances, an MIMO array will lead to the same net capacity. When moving to above 100 GHz frequency ranges, these kinds of MIMO architectures will pose a strong demand on the phase coherence for the analogue array front ends. This demand is translated into requirements of stability and linearity of the active devices, which is typically not achievable with high-frequency electronics, limiting the practical data rates [19]. Moreover, OAM and LoS MIMO architectures are based on phase interference cancellation techniques to ensure the independence between the modes and, therefore, are intrinsically narrow-bandwidth and difficult to implement at high frequencies.

In this work, instead, we study the feasibility of a different MIMO array architecture, which could be combined with wide spectral bandwidth front ends, for potential application in 220–320 GHz band, where the received signal by each of

Manuscript received 5 October 2020; revised 2 February 2022; accepted 5 March 2022. Date of publication 25 April 2022; date of current version 8 September 2022. This work was supported by the European Research Council Starting Grant ERC-2014-StG LAA-THz-CC under Grant 639749. *(Corresponding author: Shahab Oddin Dabironezare.)*

The authors are with the THz Sensing Group, Microelectronics Department, Delft University of Technology, 2628 CD Delft, The Netherlands (e-mail: n.llombartjuan@tudelft.nl; dabironezare.shahab@ieee.org).

Color versions of one or more figures in this article are available at https://doi.org/10.1109/TAP.2022.3168724.

Digital Object Identifier 10.1109/TAP.2022.3168724

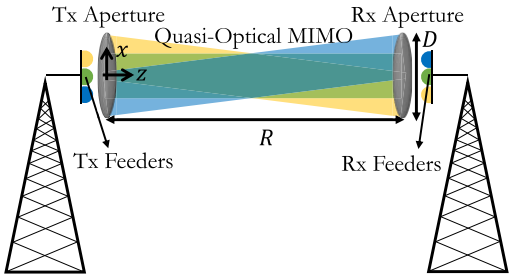

Fig. 1. Illustration of a QO MIMO system with multiple wideband radiative near-field modes. This architecture leads to spatially multiplexed data stream generated/detected by transmitting/receiving apertures coupled to two antisymmetrical Tx and Rx FPAs with respect to the z-axis. Different colors are used to illustrate the spatial near-field modes.

the array elements can be treated directly as an independent data stream (see Fig. 1), without the need of further signal processing or precoding techniques. For this purpose, we study the potential capacity and link budget when electrically large apertures are combined with single beam per element focal plane arrays. Unlike the work in [20] which investigated the capacity of THz links at far-field distances using Friis equation, here, we consider links operating in the radiating near field of electrically large apertures. Indeed, link distances within a few 100 m can be effective in the radiative near field and, therefore, the active energy can be focalized leading to negligible propagation spreading losses. The use of electrically large antennas operating in the radiative or Fresnel near-field region has been widely proposed for enabling high efficiency in wireless power transfer applications [21]–[23]. Another great advantage of the proposed near-field link is the large spatial multiplexing capability [11]. Multiple spatial and independent electromagnetic near-field modes can be generated and received via quasi-optical (QO) antennas composed of a focusing component such as a lens or reflector fed by a focal plane array. The generation and detection of the MIMO signals can be achieved via a single feed per beam focal plane configuration, where the main field coherence comes from a QO antenna and, therefore, incoherent array architectures can be used, as a contrary for OAM or LoS MIMO implementations.

By implementing an analysis of the antennas in reception [24], [25] combined with a near-field propagation, we analyze the coupling and crosstalk between the multiple elements of the transmitter and receiver arrays as a function of the antenna diameter and link distance. It is found that QO MIMO architectures based on 16 incoherent transmitters and 16 incoherent receivers could be generated over the 70 GHz bandwidth of the IEEE 802.15.3d standard. The achieved signal-to-interference ratio (SIR) is better than 17 dB for 100 m distances and 1 m apertures with only of -3 dB of power spreading for each data stream without the need for interference cancelation techniques. Combining this antenna architecture with wideband 270 GHz front ends [26]–[29] could enable PtP wireless links with aggregated capacity in the order of Tbps. The achieved MIMO capacity gain is also compared with a classical LoS MIMO architecture. An implementation of the proposed QO MIMO architecture based on reflector antennas is also simulated with a commercial software to validate the theoretical study.

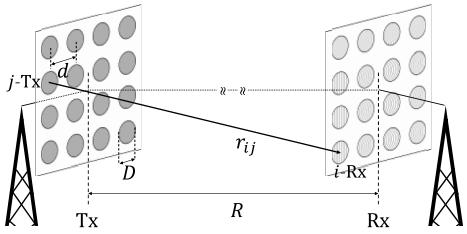

Fig. 2. Illustration of an $M \times M$ LoS MIMO system with a set of $M = 4 \times 4$ transmit and receive antenna elements separated by a link distance R.

This article is structured as follows. Section II reviews a standard LoS MIMO system and defines the benchmarks for comparing the QO MIMO to the LoS one. In Section III, the analysis methodology and achieved power coupling coefficients for radiative near-field LoS links are described. Sections IV and V discuss the spatial multiplexing capabilities of QO MIMO architectures using single or multi-near-field coherent apertures, respectively. In Section VI, one specific QO MIMO architecture is validated using commercial simulation software and its bandwidth performance is investigated. Concluding remarks are given in Section VII.

II. LoS MIMO Systems

Let us start by considering a standard LoS MIMO system. The system is composed of a transmitter and a receiver where each consists of a $M = N \times N$ square grid array, as depicted in Fig. 2. Narrow-band MIMO systems have been addressed in numerous publications with the following standard formulation of the input–output signal relationship in complex baseband notation [18]:

$$\boldsymbol{y} = \boldsymbol{H}\boldsymbol{x} + \boldsymbol{n} \tag{1}$$

where $\boldsymbol{x}$ and $\boldsymbol{y}$ are the input and output signal, respectively, for each antenna element in Fig. 2; $\boldsymbol{H}$ is the MIMO channel matrix, and the vector $\boldsymbol{n}$ represents the additive receiver noise. The channel capacity of the MIMO system can be derived as introduced by Telatar [30]. One can use a singular value decomposition (SVD) of the channel matrix

$$\boldsymbol{H} = \boldsymbol{U}\boldsymbol{\Sigma}\boldsymbol{V}^{\boldsymbol{H}} \tag{2}$$

where $\boldsymbol{U}$ and $\boldsymbol{V}$ are the unitary matrices containing the left and right singular vectors of $\boldsymbol{H}$, respectively, while $\boldsymbol{\Sigma}$ is a diagonal matrix with the positive singular values μ_i with $i = 1$ to M, in decreasing order. Equation (1) can also be expressed in the beamspace [31] as follows:

$$\tilde{\boldsymbol{y}} = \boldsymbol{U}^{\boldsymbol{H}}\boldsymbol{H}\boldsymbol{V}\tilde{\boldsymbol{x}} + \boldsymbol{U}^{\boldsymbol{H}}\boldsymbol{n} = \boldsymbol{\Sigma}\tilde{\boldsymbol{x}} + \tilde{\boldsymbol{n}} \tag{3}$$

where $\tilde{\boldsymbol{x}}$ and $\tilde{\boldsymbol{y}}$ correspond directly to the input/output signals associated with each MIMO data stream and $\boldsymbol{V}$ and $\boldsymbol{U}^{\boldsymbol{H}}$ are the beamforming matrices for the transmit and received arrays, respectively. In our comparative study, we would assume

that the amplitude and phase weights of these beamforming matrices are realizable at any range.

The corresponding capacity of the MIMO system becomes

$$C_{\mathrm{MIMO}} = \sum_{i=1}^{M} \log_2\left(1 + \mathrm{SNR}_{\mathrm{SISO}} \frac{\mu_i^2}{M}\right) \tag{4}$$

where $\mathrm{SNR}_{\mathrm{SISO}} = S_0/N_0$ is the received signal, S_0, to noise, N_0, ratio of the corresponding single input single output (SISO) link assuming that all the available power is distributed across the MIMO links. It is common to then define a MIMO capacity gain as follows:

$$G_{\mathrm{MIMO}} = \frac{C_{\mathrm{MIMO}}}{\log_2(1 + \mathrm{SNR}_{\mathrm{SISO}})} \tag{5}$$

where the achieved MIMO capacity is benchmarked with that of the SISO link.

The optimization of LoS MIMO systems has been widely based on the assumption of far-field links where the channel matrix is modeled using phase delays as follows:

$$h_{ij} = e^{-\mathrm{j}kr_{ij}} \tag{6}$$

where h_{ij} is an element of the MIMO channel matrix H, with r_{ij} being the distance between the ith receiver and the jth transmitter (see Fig. 2), and k is the propagation constant. The received power is evaluated using the Friis equation

$$P_{\mathrm{Rx}}^{\mathrm{far}} = P_{\mathrm{Tx}} G^2 \left(\frac{\lambda}{4\pi R}\right)^2 \tag{7}$$

where P_{Tx} is the transmitted power, G is the antenna gain of a single element of the array in Fig. 2, and R is the link distance. Under these assumptions, the channel matrix H is unitary and the optimal array spacing becomes $d = \sqrt{\lambda R/N}$ leading to a MIMO capacity gain of $G_{\mathrm{MIMO}} = N \times N = M$ since the interference or crosstalk between the data streams is fully cancelled. For this optimal array spacing and specific range distance, precoding techniques based on quadrature phase shifters have been proposed in the millimeter-wave band to simplify the beamforming implementation [32]. However, the difficulties on implementing precoding techniques increases significantly with frequency [33].

Equation (6) only holds when the link distance R is larger than the far-field Rayleigh limit considering the entire array aperture [i.e., $R > 2(N-1)^2 d^2/\lambda$]. This condition is only verifiable for 4×4 LoS MIMO configuration when the aperture size of the array elements, D, is much smaller than d. For other configurations with $N > 2$, the amplitude of the channel matrix elements will not be any more equal to 1 but altered by the radiation pattern of the array elements as follows:

$$h_{ij} = \left|E_0(\theta_{ij})\right|^2 e^{-\mathrm{j}kr_{ij}} \tag{8}$$

where $E_0(\theta_{ij}) \leq 1$ is the normalized radiation pattern of the array elements from Fig. 2. For the sake of simplicity, all the elements are considered to be the same and radiating rotationally symmetric fields. The angle θ_{ij} corresponds to the subtended θ-angle between the ith transmitter and jth receiver. Equation (8) is now valid as long as R is larger than the far-field Rayleigh limit considering the aperture size of the elements (i.e., $R > 2D^2/\lambda$). Similar steps described before can be performed to derive the MIMO capacity as in (4). In this work, we model the transmitting and receiving antennas using equivalent electric field aperture distributions [34] with the following expression:

$$\vec{E}_{\mathrm{ap}}(\rho) = E_0 \mathrm{circ}\left(\rho, \frac{D}{2}\right) e^{-\frac{\rho^2}{w_0^2}} \hat{x} \tag{9}$$

where circ function indicates a circular aperture domain with the diameter D, ρ is the radial position on the aperture, $\hat{x}$ refers to an x-polarized electric field, and $w_0 = 0.44D$ is defined to achieve a -11 dB field edge taper. This expression models well the aperture distribution in front of highly directive antennas, such as parabolic reflectors or lenses. $E_0(\theta_{ij})$ in (8) is calculated by taking the Fourier transform of (9).

Let us consider an $R = 100$ m link operating at frequency of 270 GHz in line with the new IEEE H-band standard for LoS wireless applications [5]. Here, the MIMO array spacing, d, is optimized for 100 m distance. The considered configurations are a 4×4 LoS MIMO where $D = (d/1.38) = 16.67$ cm and $D = d/4 = 5.75$ cm. We assume a wide bandwidth of 35 GHz and a noise figure of 10 dB leading to -59 dBm of noise power. The total transmitted power, P_{Tx}, is -14.4 dBm for $D = d/1.38$ and 4 dBm for $D = d/4$ to compensate for the lower antenna gain in (7). To compare these geometries, we can look into the average of the signal-to-noise ratio (SNR) in decibels

$$\mathrm{SNR}_{\mathrm{ave}}^{\mathrm{dB}} = \frac{1}{M} \sum_{i=1}^{M} \mathrm{SNR}_i^{\mathrm{dB}} \tag{10}$$

where $\mathrm{SNR}_i = \mathrm{SNR}\mu_i^2/M$. Since the capacity of a MIMO system, (4), scales logarithmically with SNR, average SNR in dB is chosen as a parameter to represent the performance of the considered MIMO systems. Fig. 3(a) and (b) shows $\mathrm{SNR}_{\mathrm{ave}}^{\mathrm{dB}}$ and G_{MIMO}, respectively, for both cases and the corresponding SISO case as a function of the link distance. We assume that the MIMO beamforming matrices for the transmit and received arrays, as in (3), are applied specifically for each considered distance based on the channel matrix evaluation for that specific distance. The SISO spectral capacity is 9.47 bit/Hz/s at 100 m. It can be seen that for the smaller D case, the results achieved using (8) are very closed to the ideal case evaluated using (6). However, the penalty is the much higher level of transmitted power which is difficult to obtain at high frequencies. Fig. 3(a) and (b) shows the results as well for a 16×16 LoS MIMO where $D = d = 16.67$ cm and $P_{\mathrm{Tx}} = -20$ dBm. In this case, the SISO spectral capacity is 7.47 bit/Hz/s at 100 m. Here, a larger difference is seen between the results obtained using the ideal channel model and the one including the effect of the antenna patterns. Even so, the MIMO gain is high, 12.7, leading to a MIMO spectral capacity of 94.86 bit/Hz/s higher than the one of the 4×4 MIMO system with 31.81 bit/Hz/s for the same power transmitted.

The difficulty in implementing these types of LoS MIMO systems, especially at high frequencies, is the need for very

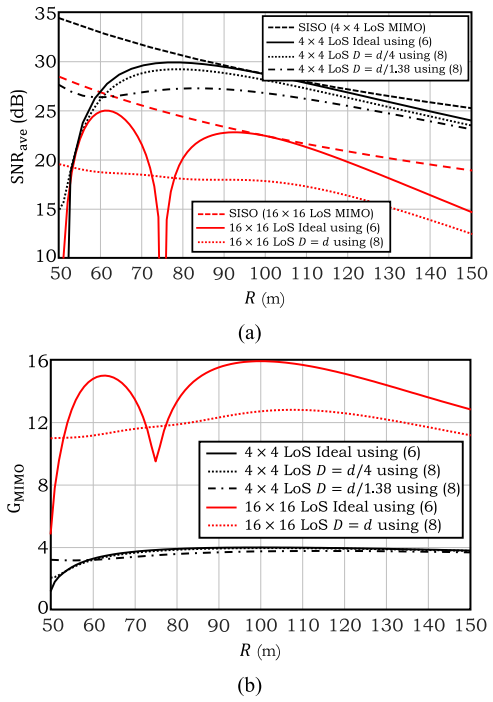

Fig. 3. (a) Average SNR, as defined in (10), for 4 × 4 and 16 × 16 LoS MIMO systems compared with one of their corresponding SISO systems. (b) MIMO capacity gain, as defined in (5), for the same cases of (a). The LoS MIMO array spacing is optimized for $R = 100$ m distance using the expression $d = \sqrt{\lambda R/N}$. The MIMO beamforming matrices for the transmit and received arrays, as in (3), are applied for each considered distance.

accurate interference cancellation techniques. In the following, we will introduce a different type of MIMO architecture, referred here as QO-MIMO, where the aim is to generate an MIMO channel matrix that is close to diagonal to remove the need for the phase coherency or precoding techniques. The idea is to generate low crosstalk between multiple data streams by exploiting the large amplitude variations in the radiative near field combined with beamforming using a QO antenna.

III. Radiative Near-Field LoS Link

At high frequencies, it is possible to realize extremely high antenna gains with moderate physical dimensions. For a few hundred meters, it is possible to operate LoS links, as shown in Fig. 1, in the radiative near field, where the Friis equation would not be applicable. In this section, we describe a methodology based on antennas in reception to evaluate the MIMO's channel matrix as well as its SNR when the LoS link is in the radiative near field.

The near field radiated by an aperture field described in (9) can be evaluated using the radiative components of the free space Green's function as follows:

$$\vec{E}^{\mathrm{Tx}}(\vec{r}) = 2\iint_{S'} \mathrm{j}\vec{k} \times \left(-\hat{z}\times\vec{E}_{\mathrm{ap}}\left(\vec{r}'\right)\right)\frac{e^{-\mathrm{j}k|\vec{r}-\vec{r}'|}}{4\pi|\vec{r}-\vec{r}'|}dS' \quad (11)$$

where $\vec{r}$ and $\vec{r}'$ indicate the vectorial position of the observation points and the source points (transmit aperture), respectively; $\vec{k} = k((\vec{r}-\vec{r}')/(|\vec{r}-\vec{r}'|))$ is the propagation vector, k is the propagation constant, and S' is the surface of the transmit aperture.

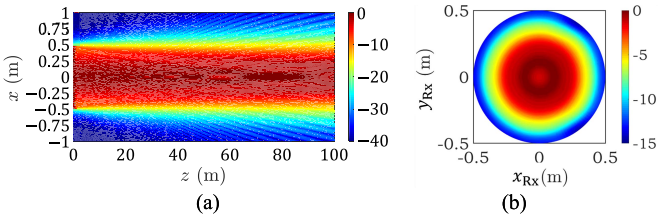

Fig. 4. Magnitude of the x-component of the electric field radiated by an aperture of 1 m diameter, evaluated on (a) xz plane (see Fig. 1) and (b) xy plane at a distance of $R = 100$ m. The aperture is focusing at infinity (corresponding to a parabolic reflector).

Fig. 4(a) shows the electric field radiated by an aperture of diameter 1m for a link distance of $R = 100$ m. It can be seen that a high power transfer can be achieved in this case. The corresponding transmitted field evaluated over the receiving aperture is shown in Fig. 4(b), showing again the high focusing capacity of these large apertures.

In order to evaluate the coupling between two antennas in the near field, we apply a similar approach as in [25] based on the analysis of antennas in reception. The induced open-circuit voltage, V_{oc}, on the receiving antenna can be evaluated as follows:

$$V_{\mathrm{oc}} I_0 = \frac{2}{\zeta_0}\iint_{A_{\mathrm{Rx}}} \vec{E}^{\mathrm{Tx}}\cdot\vec{E}^{\mathrm{Rx}}_{\mathrm{ap}}dS \quad (12)$$

where ζ_0 is the free space impedance, $\vec{E}^{\mathrm{Tx}}$ is the transmitted field evaluated on receiving aperture, A_{Rx}, and $\vec{E}^{\mathrm{Rx}}$ is the field radiated by the receiver (when operated in transmission fed by a current I_0) evaluated on the receiving aperture, which for the present work is modeled by (9). The power coupling coefficient ($S_{\mathrm{TxRx}} \leq 1$) between the two apertures can then be evaluated from this induced voltage as follows:

$$S_{\mathrm{TxRx}} = \frac{|V_{\mathrm{oc}} I_0|^2}{16 P_{\mathrm{Tx}} P_{\mathrm{Rx}}} \quad (13)$$

where $P_{\mathrm{Tx/Rx}} = (1/(2\zeta_0))\iint_{A_{\mathrm{Tx/Rx}}} |\vec{E}^{\mathrm{Tx/Rx}}_{\mathrm{ap}}|^2 dS$ (valid only for electrically large antennas), and $A_{\mathrm{Tx/Rx}}$ represents the transmitting/receiving aperture. Therefore, the channel voltage coefficient between transmitter j and receiver i can be expressed as follows:

$$h_{ij} = \frac{\iint_{A_{\mathrm{Rx}}} \vec{E}^{\mathrm{Tx},i,j}\cdot\vec{E}^{\mathrm{Rx},i}_{\mathrm{ap}}dS}{\sqrt{\iint_{A_{\mathrm{Tx}}} |\vec{E}^{\mathrm{Tx},j}_{\mathrm{ap}}|^2 dS}\sqrt{\iint_{A_{\mathrm{Rx}}} |\vec{E}^{\mathrm{Rx},i}_{\mathrm{ap}}|^2 dS}}. \quad (14)$$

This equation is similar to the one derived by other authors to evaluate the crosstalk between the beams radiated by a single antenna [35] but used here to evaluate the near-field coupling between the transmit and receive antennas. When the antennas are in the far-field distance of each other, (14) simplifies to (8). From these expressions, it is clear that the power transferred is maximized, when $\vec{E}^{\mathrm{Rx}}_{\mathrm{ap}} = \vec{E}^{\mathrm{Tx}*}$ and the spill over between the two antennas is low, leading to $S_{\mathrm{TxRx}} = 1$. Fig. 5(a) and (b) shows the amplitude and phase of $\vec{E}^{\mathrm{Tx}}$ and $\vec{E}^{\mathrm{Rx}}_{\mathrm{ap}}$, respectively, for the same case as in Fig. 4. Here, a very high power coupling coefficient S_{TxRx} of -0.3 dB is

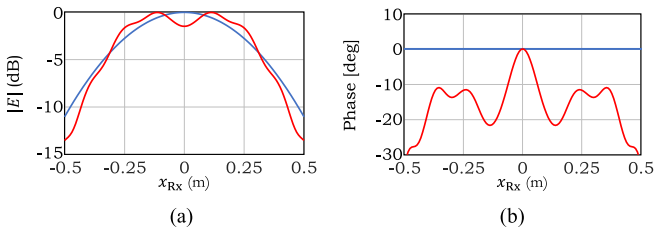

Fig. 5. Field matching between the transmitted fields, red colored curves, and receiving aperture field distribution, blue colored curves, for the same case as in Fig. 4. (a) Amplitude matching. (b) Phase matching.

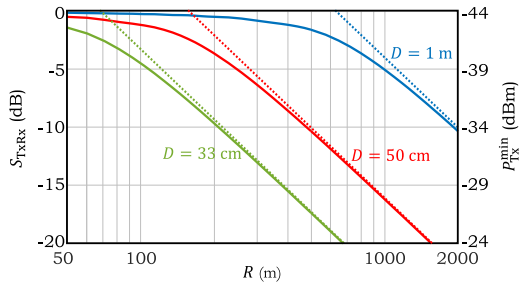

Fig. 6. Near, solid lines, and far field (Friis equation), dashed lines, coupling coefficients between two co-aligned antennas of diameter D with separation distance R. The right axis represents the minimum transmitted power required to reach an SNR = 15 dB, assuming a receiver noise level of −59 dBm.

achieved. We have observed similar coupling coefficient when the transmitting aperture focuses the energy at the middle of the link (corresponding to an elliptical reflector) as investigated in [21]. However, since the phase configuration with a focus at infinity is more robust toward changes in the link distance, we only consider here these type of aperture distributions.

A similar analysis can now be performed versus the link distance and considering different aperture diameters. Fig. 6 shows the achieved coupling coefficients for such analysis. It can be seen that for $D = 50$ cm, corresponding to far-field directivities of 62 dBi, power couplings above −5 dB can be achieved for distances less than 300 m, whereas $D = 1$ m leads to much larger distances for comparable level of coupling coefficients. On top of these curves, we also plotted the coupling coefficient derived directly from the Friis equation (7). The two coupling coefficients become equivalent when the far-field boundary $R > 2D^2/\lambda_c$ is reached. Here, λ_c is the free space wavelength at the center of the frequency band (270 GHz).

By considering the coupling coefficients shown in Fig. 6, it is clear that the use of electrically large apertures leads to the need for very low levels of transmitted power. As an example, let us consider an RF channel of 35 GHz (half of the available bandwidth in IEEE standard) and a minimum SNR of 15dB (needed for 16QAM modulation schemes with bit error rate BER = 10^{-6} [36]). Under these hypotheses, single wideband data stream with speeds reaching 80 Gb/s[1] could be potentially implemented. By using the coupling coefficients, S_{TxRx}, in Fig. 6, we can estimate the minimum transmit power level required to establish such single channel link as follows:

$$P_{\text{Tx}}^{\min}\ (\text{dBm}) > \text{SNR} - S_{\text{TxRx}} + N\ (\text{dBm}) \tag{15}$$

where the noise is estimated to be N (dBm) = −59 dBm[2] assuming a receiver with 10 dB of noise figure [20]. The right vertical axis in Fig. 6 shows the achieved $P_{\text{Tx}}^{\min}$. Very low levels of transmitted powers would be indeed required, simplifying the active circuity implementation at high frequencies and enabling radiated energy efficient systems. In the literature, several demonstrations of a single far-field link reaching 100 Gbps have already been demonstrated in this spectral band [26]–[29] with transmitted power levels in the order of −8 to 5 dBm.

IV. Spatial Multiplexing via Single Near-Field Coherent Aperture

A significant advantage of operating a wireless link in the radiative near field is the high degree of spatial multiplexing capabilities for PtP links [11]. Several data streams can be generated with low coupling relying only on the spatial shape of the electromagnetic near field generated at the receiving aperture by a QO antenna. This antenna can be easily implemented with an electrically large aperture and a focal plane array. The transmitting focal plane array can be operated as a single data stream per element, common architecture at high frequencies, [37], [38], avoiding the need for high linearity circuits or coherent array implementations. The receiving array is made by an anti-symmetrical, with respect to the z-axis, implementation of the transmitting focal plane array to achieve a field matched in (12) for each of the near-field modes. The receiving focal plane array, also implemented as a data stream per element, will then be well-coupled to each of the independent data streams sent by the transmitting array. In all the cases considered in this work, the location of the receiving and transmitting focal plane antennas is physically fixed, i.e., they are not varied with respect to range or frequency values.

Fig. 1 shows the proposed QO MIMO transmit and receive architectures: two anti-symmetrical $N \times N$ focal plane arrays enable $M = N^2$ near-field spatial beams, potentially increasing the aggregated data rate by a factor of $\sim M$. On top of these near-field spatial modes, polarization diversity can be used to increase the aggregated data rate by an additional factor of 2 since the QO MIMO multiplexing capabilities presented here do not rely on polarization orthogonality.

In order to model each of the aperture fields associated with the multiple elements of the Tx and Rx focal plane arrays, we use the following expression:

$$\vec{E}_{\text{ap}_n}^{\text{Tx/Rx}}(\rho) = E_0 \text{circ}\left(\rho, \frac{D}{2}\right) e^{-\frac{\rho^2}{w_0^2}} e^{\text{j}k\frac{\vec{\rho}_n^{Tx/Rx}\cdot\vec{\rho}}{F}}\hat{x} \tag{16}$$

where n indicates the considered element in the FPA. The last term corresponds to a linear phase shift associated with the displacement of the nth-element from the focus of the QO antenna, characterized with a focal distance of F. This phase shift is related to the f-number $f_\# = F/D$ of the QO antenna and the number of displaced beams, as follows:

$$\vec{\rho}_n^{\text{Tx/Rx}} = n\lambda_c f_\# \hat{\rho}_n^{\text{Tx/Rx}} \tag{17}$$

[1]0.2 roll-off is assumed.

[2]The noise level is evaluated as $k_B T_0 FBW$.

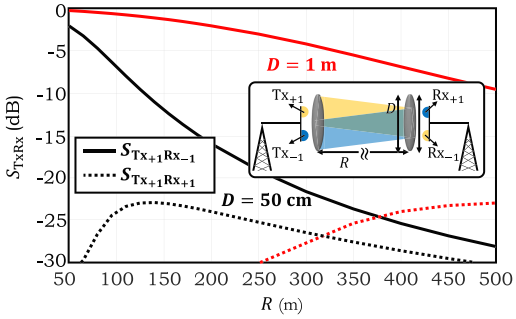

Fig. 7. Co- and cross-coupling coefficients versus the link distance between different elements of transmitting and receiving FPAs with 2 × 1 elements. The inset illustrates the position of the feeds in the Tx and Rx FPAs.

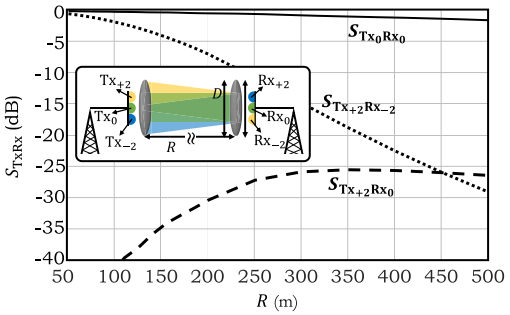

Fig. 8. Co- and cross-coupling coefficients versus the link distance between different elements of transmitting and receiving FPAs with 3 × 1 elements and $D = 1$ m. Inset: Position of the feeds in the Tx and Rx FPAs.

where $\hat{\rho}_n^{\mathrm{Tx/Rx}}$ is the unit vector indicating the ϕ-plane of nth element displacement. The linear phase term in (16) can be related directly to the number of scanned beams (i.e.,$n(\lambda_c/D)$) independently of the focal distance F as follows:

$$e^{\mathrm{j}k\frac{\vec{\rho}_n^{\mathrm{Tx/Rx}}\cdot\vec{\rho}}{F}} = e^{\mathrm{j}k\frac{n\lambda_c}{D}\hat{\rho}_n^{\mathrm{Tx/Rx}}\cdot\vec{\rho}}. \tag{18}$$

Therefore, the proposed implementation, in a first-order approximation, is not dependent on $f_\#$ of the QO antennas.

Let us now consider an FPA of 2 elements in both the Tx and Rx antennas displaced by $n = \pm 1$ in the x plane, see inset of Fig. 7. Note, as shown in Fig. 1, the elements with maximum coupling are mirrored with respect to the z-axis at the receiver side. The distance between the array elements is considered $2\lambda_c f_\#$ to avoid direct beam coupling [39] and be able to exploit dual-polarized elements also as means for channel diversity. The co- and cross-coupling power coefficients, $S_{\mathrm{Tx}_m\mathrm{Rx}_n}$, associated with one transmitter at $m = +1$ and the power received by each of the receiving elements, $n = \pm 1$, can be evaluated using the same approach as in (12) projecting the transmitted field into the multiple receiving aperture fields of (16). The resulting values are shown in Fig. 7. It can be seen that co to cross ratios (also commonly referred to as signal to interference level) larger than 20 dB can be achieved up to 350 m distance for 1 m apertures or up to about 70 m for 50 cm apertures. In both cases, the possibility of multiplexing several data streams corresponds to ranges where the co-coupling coefficients are higher than −5 dB.

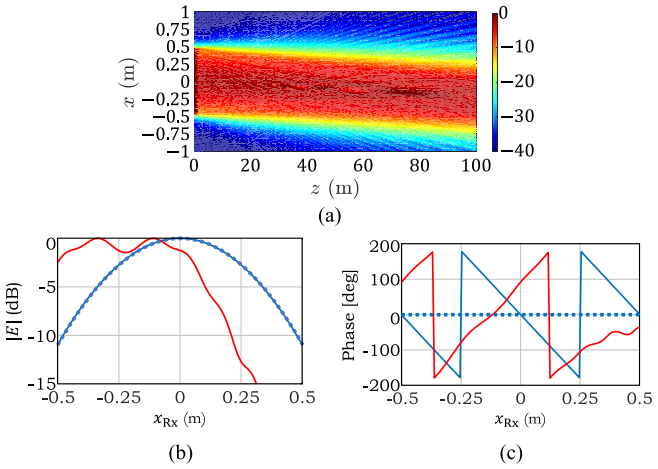

Fig. 9. (a) Near field radiated by an aperture of 1 m fed by an element located at $+2\lambda_0 f_\# \hat{x}$ and evaluated in the xz plane. Field matching between the transmitted fields (solid red curves) evaluated at $R = 100$m on the Rx aperture and the receiving aperture field distributions (blue curves), (b) amplitude matching, and (c) phase matching. The solid blue and dotted blue curves correspond to the receiving aperture field distribution for a feed element located at $-2\lambda_c f_\# \hat{x}$ and the one at the center of the aperture, respectively.

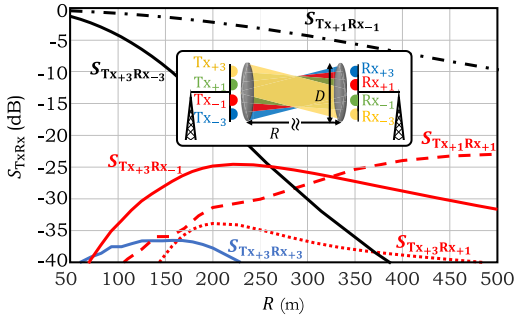

Fig. 10. Co- and cross-coupling coefficients versus the link distance between the different elements of transmitting and receiving FPAs of 4 × 1 elements and $D = 1$ m. The inset illustrates the position of the feeds in the Tx and Rx FPAs.

It is also possible to multiplex more data streams for $D = 1$ m case at shorter ranges. Let us consider Tx and Rx arrays of three elements placed at m and $n = [0, \pm 2]$, see inset of Fig. 8. Fig. 8 also shows the coupling and cross-coupling coefficients between these three near-field modes. Co-coupling levels higher than −5 dB in the off axes elements, $S_{\mathrm{Tx}_{+2}\mathrm{Rx}_{-2}}$, can be reached up to 150 m, whereas co/cross ratios larger than 20 dB can be achieved up to 200 m. Fig. 9(a) shows the field propagation in the xz cut for $R = 100$ m associated with the $m = +2$ transmitting element. This element has a co-coupling coefficient of $S_{\mathrm{Tx}_{+2}\mathrm{Rx}_{-2}} = -2$ dB with the $n = -2$ receiving array element, and a cross-coupling coefficient with neighbor receiving array element, $n = 0$, of $S_{\mathrm{Tx}_{+2}\mathrm{Rx}_0} = -41$ dB. Fig. 9(b) and (c) shows the amplitude and phase of $\vec{E}_{\mathrm{Tx}}$ and $\vec{E}_{\mathrm{ap}}^{\mathrm{Rx}}$ for the same cases as in Fig. 9(a).

Finally, let us consider FPAs of four elements placed at m and $n = [\pm 1, \pm 3]$ along x, see inset of Fig. 10. Fig. 10 also shows the resulting coupling and cross-coupling between the 4 array elements. Co-coupling levels higher than −5 dB in

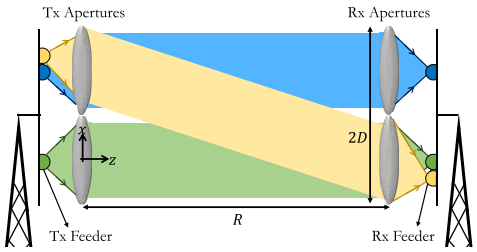

Fig. 11. QO MIMO architecture for multiplexing data streams in the radiative near-field composed by multiple transmitting and receiving apertures coupled to antisymmetrical Tx and Rx FPAs with respect to the z-axis.

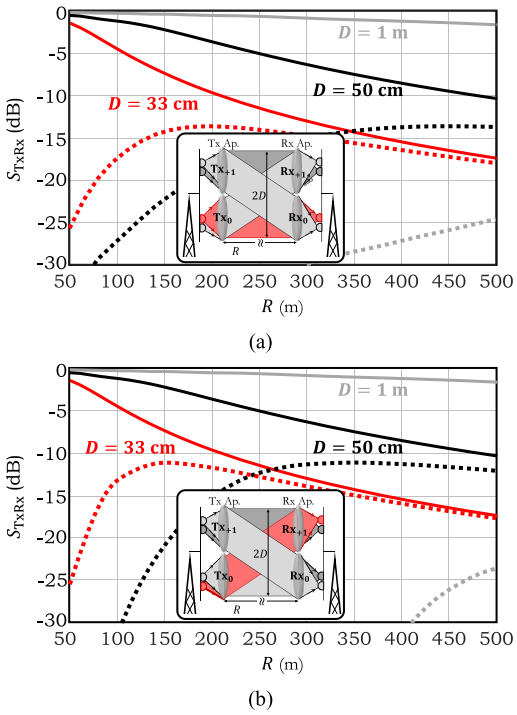

Fig. 12. Co, solid lines, and cross-coupling, dotted lines, coefficients versus the link distance in the configuration shown in Fig. 11 for (a) on-axis feeds and (b) off-axis feeds. The insets illustrate the position of the feeds inside each Tx and Rx apertures where the co-channels are marked by red color.

the off-axes elements, $S_{\mathrm{Tx}_{-3}\mathrm{Rx}_{+3}}$, and co/cross ratios larger than 20 dB can be achieved up to 120 m. The limiting factor here is the rapid decay for the co-coupling of the off-set focal plane elements.

V. Spatial Multiplexing via Multiple Near-Field Incoherent Apertures

It is also interesting to analyze a different QO antenna configuration, where the main aperture is divided into several coherent apertures shown in Fig. 11, as in a Fly's eye lens array [25]. This antenna architecture is much easier to fabricate and integrate with multiple signal generation schemes at high frequencies because of the larger space of the transmitting and receiving feed antennas.

Let us consider an overall aperture diameter of 1m that can be divided into 2 × 2 apertures of 50 cm each or 3 × 3 apertures of 33 cm each, leading to potential multiplexing of 4 or 9 near-field modes, respectively. Fig. 12(a) shows the

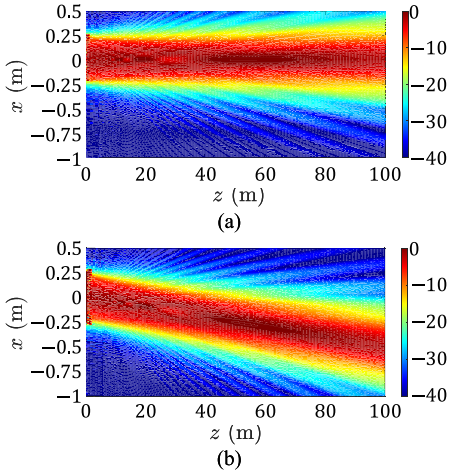

Fig. 13. Near field radiated in the xz plane by an aperture of 50 cm (a) with an on-axis feed (blue colored link in Fig. 11) and (b) with off-axis feed located at $+2.25\lambda_c f_{\#}\hat{x}$ (yellow colored link in Fig. 11).

co-coupling between the two of these apertures with on-axis feeds (blue or green colored near-field modes in Fig. 11) and its cross-coupling with the other elements. The procedure to evaluate these couplings is analogous as before. It can be seen that in order to achieve co/cross >20 dB, $R < 150$ m for the 50 cm case and $R < 66$ m for the 33 cm case. The field generated by a 50 cm aperture is shown in Fig. 13(a). The range distance with a low cross-coupling is indeed smaller for a comparable multiplexing capability achieved with a single 1 m antenna, as indicated in Figs. 7 and 8. However, the practical implementation of this second configuration is easier due to the smaller coherent aperture size, and the antennas could be potentially aligned independently by implementing defocus feeds as in [40]. Moreover, this architecture could evolve in the future toward hybrid QO and LoS MIMO implementations to exploit some degree of coherence between the array elements and reach larger distances as the performance of the high-frequency technology improves.

The multiplexing capabilities of a single 50 cm aperture with 2 × 2 FPA are not sufficient to reach co/cross ratios of >20 dB at 100 m, as shown in Fig. 7. However, 2 × 2 FPA implementations can also be combined with the 2 × 2 50 cm aperture configuration as in Fig. 11 to enable new near-field links that couple between the different apertures (yellow colored link). Let us consider that a second feed is placed at the top 50 cm aperture at $2.25\lambda_c f_{\#}$ distance from the center of the FPA. This feed will not couple to the top aperture, but it will couple to the bottom one. The field generated by such feed is shown in Fig. 13(b). Fig. 12(b) shows the co-coupling between two apertures with off-axis feeds (yellow colored link in Fig. 11) and its cross-coupling with the other elements. As it can be seen, the co-coupling levels for the off-axis feeds are comparable with the ones of the on-axis channel, while the cx-couplings are about 2–3 dB higher in the off-axis channels.

A. 16 × 16 QO-MIMO Architecture

Let us now consider a constant link distance of 100 m, where we could potentially multiplex up to 16 data streams.

TABLE I

CO- (GREEN CELLS) AND CROSS-COUPLING COEFFICIENTS IN DECIBEL (ROUNDED) FOR A 16 × 16 TX/RX ARRAYS OF FIG. 14: IN-HOUSE ANALYSIS CODE/IMPLEMENTATION IN GRASP (FIG. 16)

$Tx^{i,j}_{m,n}$ / $Rx^{i,j}_{m,n}$	0,0 0,0	+1,0 +1,0	0,+1 0,+1	+1,+1 +1,+1	0,+1 0,0	0,+1 −1,0	0,0 0,−1	0,+1 −1,+1	+1,0 0,0	0,0 −1,0	+1,0 0,−1	+1,0 +1,−1	+1,+1 0,0	+1,+1 +1,0	+1,+1 0,+1	0,0 −1,−1	Tot. Int.	SIR
0,0 0,0	-1/-2	-31/-33	-31/-33	-45/-45	-27/-28	-49/-49	-31/-31	-52/-54	-27/-28	-31/-31	-49/-49	-52/-54	-45/-46	-49/-50	-49/-50	-45/-43	-21/-22	20/20
0,0 −1,0	-31/-31	-1/-2	-45/-43	-31/-32	-49/-49	-70/-70	-52/-53	-51/-51	-31/-31	-43/-44	-45/-43	-31/-31	-49/-49	-27/-28	-52/-55	-51/-51	-23/-23	22/21
0,0 0,−1	-31/-31	-45/-44	-1/-2	-31/-32	-31/-32	-45/-43	-43/-44	-31/-31	-49/-49	-52/-53	-69/-72	-51/-51	-49/-50	-52/-55	-27/-28	-51/-51	-23/-23	22/21
0,0 −1,−1	-45/-43	-31/-31	-31/-31	-1/-2	-52/-54	-51/-51	-51/-51	-43/-44	-52/-54	-51/-51	-51/-51	-43/-44	-45/-44	-31/-32	-31/-31	-58/-57	-25/-25	24/23

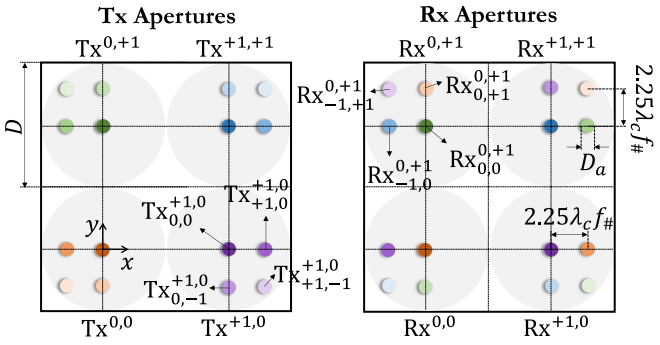

Fig. 14. 2 × 2 antenna apertures with 2 × 2 FPA configurations, each, to achieve 16 spatial data streams at 100 m.

The proposed antenna configuration is shown in Fig. 14, the Tx and Rx FPA elements will be distributed in groups of 2 × 2 arrays below each of the 2 × 2 50 cm apertures. The corresponding focal plane configurations are shown in Fig. 14. The x and y distances between elements are $2.25\lambda_c f_\#$. The transmit and receive array elements with the same color indicate co-data stream configurations. The Tx and Rx elements in this configuration are referred to as $\mathrm{Tx/Rx}^{i,j}_{m,n}$, where i, j and m, n indicate the position of the aperture and the feed element with respect to the marked xy coordinates, respectively.

Table I shows the achieved co- (h_{ii}) and cross- (h_{ij} with $i \neq j$) couplings for this QO MIMO configuration showing high and stable co-coupling levels, and low interference levels. The missing rows can be easily derived applying symmetries. Total level of signal to interference, SIR, for each channel is given in the last column. The SIR is evaluated, assuming the power in the interfering channels is added incoherently

$$\mathrm{SIR}_i = \frac{|h_{ii}|^2}{\sum_{j=1, j\neq i}^{M} |h_{ij}|^2}. \tag{19}$$

The total level of signal to interference for the proposed configuration is estimated to be about 21 dB. The achieved co-couplings for all 16 data streams in this architecture are −1 dB, much more uniform compared with the results of a single aperture from Fig. 10.

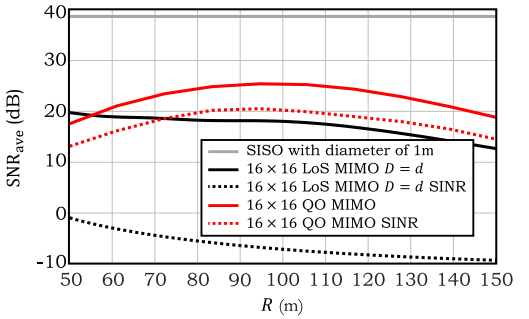

(a)

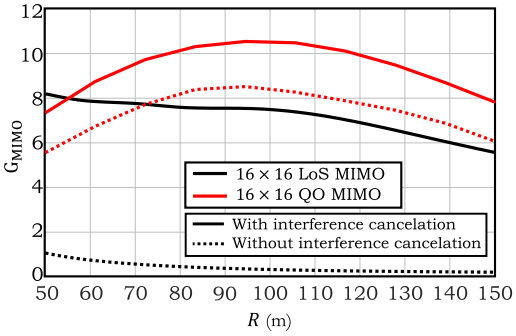

(b)

Fig. 15. (a) SNR and SINR for the standard 16 × 16 LoS MIMO and the proposed QO MIMO artitechture as a function of the link distance. (b) Capacity gain of the architectures in (a) as a function of link distance with (solid curves) and without (dotted curves) considering an interference cancellation technique based on the MIMO beamforming matrices derived in (3) for each considered distance. The capacity gain is evaluated here with an SISO reference of 1m diameter.

B. MIMO Capacity Gain

In this subsection, we evaluate the MIMO capacity gain of the proposed architecture and compare it with a standard 16 × 16 LoS MIMO (see Fig. 2). For this comparison, we chose the same SISO reference for the LoS and QO architectures. The SISO reference is taken as a single antenna with 1 m diameter to ensure that all considered cases have the same physical dimension. For the SISO reference, we take a 1 m circular aperture with −20 dBm of radiated power and −59 dBm of thermal noise. Fig. 15(a) shows the achieved SNR

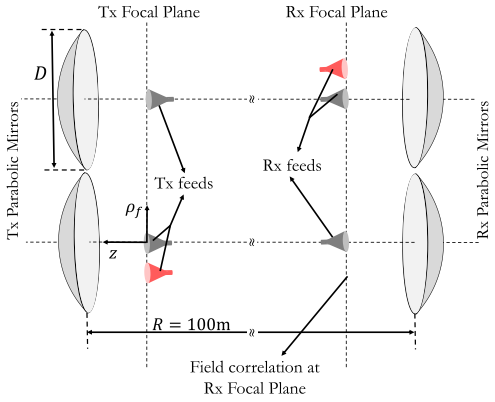

Fig. 16. 2 × 2 Paraxial apertures with Tx and Rx FPA configurations to achieve 16 data streams multiplexing at 100 m via $D = 50$ cm apertures.

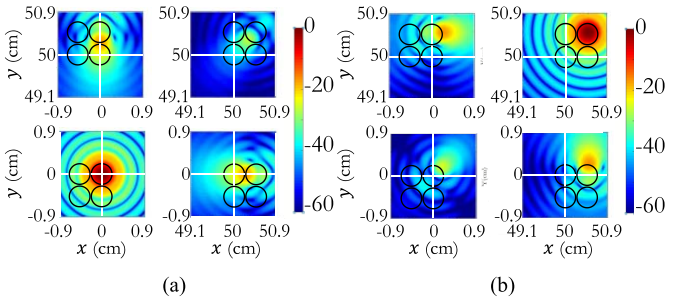

Fig. 17. Fields simulated by GRASP for (a) $Tx_{0,0}^{0,0}$ and (b) $Tx_{-1,-1}^{0,0}$ elements of Fig. 14 on the focal planes of its four receiving apertures. The black colored circles mark the position of the receiving feeds in Rx FPAs.

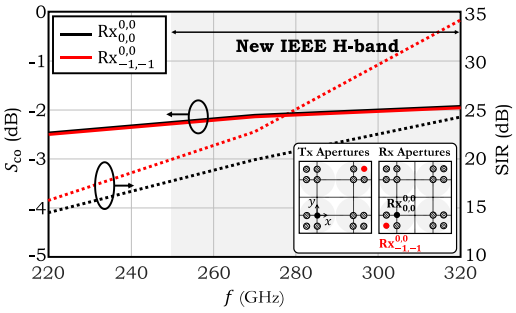

Fig. 18. Co- (solid lines) and signal to interference (dotted lines) performance for a 16 channels Tx/Rx array of Fig. 14, as a function of operation frequency. Inset: Position of the feeds in the Tx/Rx FPAs and the colored feeds indicate the two most relevant channels.

for this SISO reference with a 12.8 bit/Hz/s spectral efficiency. In Fig. 15(a), the average SNRs for the 16 × 16 LoS MIMO with $d = D$ and the proposed 16 × 16 QO MIMO, when a crosstalk cancellation technique is applied following the SVD decomposition as described in Section II, are shown. These results are obtained, assuming an ideal cancellation technique without imposing any practical constrains in terms of phase cancellation. Due to the different SISO reference here with respect to the one in Fig. 3(a), the capacity gain of the LoS MIMO shown in Fig. 15(b) is lower than the one in Fig. 3(b).

The QO MIMO achieves a better capacity gain with respect to both the 1 m SISO and LoS MIMO references. The QO MIMO achieves a theoretical spectral efficiency of 134.5 bit/Hz/s compared with the 95.42 bit/Hz/s of the LoS MIMO. Fig. 15(a) and (b) also shows the average signal-to-interference and noise ratio (SINR) and capacity gain, respectively, when no crosstalk cancellation is applied. That is directly using an incoherent array architecture. For this configuration, the QO MIMO architecture clearly outperforms the standard LoS MIMO architecture leading to a theoretical spectral capacity of 106 bit/Hz/s with respect to 3.84 bit/Hz/s.

VI. Example of Implementation

In this section, we validated the proposed QO MIMO antenna architecture using a commercial software (GRASP [41]) and a standard reflector antenna implementation. Fig. 16 shows the considered geometry made of four co-aligned parabolic reflectors with $f_\# = 2$. These reflectors are fed by tapered circular feed apertures which model the aperture field of a horn or lens antenna [39] as follows:

$$\vec{E}_{\text{feed}}(\vec{\rho}_f) = E_0 \text{circ}(\rho_f, D_a/2) e^{-\frac{\rho_f^2}{w_f^2}} \hat{x} \tag{20}$$

where w_f is chosen in such a way to have a field taper level of −8 dB at the feed aperture to achieve an illumination of the reflector with an edge taper field level of −11 dB with a feed aperture of diameter $D_a = 2\lambda_c f_\#$; $\vec{\rho}_f$ represents the radial position in the focal plane (Fig. 16). The fields generated by $\text{Tx}_{0,0}^{0,0}$ and $\text{Tx}_{-1,-1}^{0,0}$ array elements (see Fig. 14) in the focal plane of the receiving reflectors are plotted in Fig. 17(a) and (b), respectively. It can be observed that the maximum coupling with these fields occur for $\text{Rx}_{0,0}^{0,0}$ and $\text{Rx}_{+1,+1}^{+1,+1}$, respectively, as anticipated previously. The low cross-coupling is achieved thanks to the spatial distribution of the field generated in the focal plane by the QO antenna implementation. The power coupling can be evaluated as in (13), where the field correlation is performed over the focal plane of the receiving apertures between the field simulated in GRASP, Fig. 17, and the field distribution of the receiving feeds (20).

Table I also shows the achieved co- and cross-coupling for this configuration using the fields evaluated in GRASP, showing comparable signal to interference levels to the ones simulated with in-house code. The co-coupling levels are about 0.9 dB lower due to two times the reflector spill over losses. The spill over loss of these feeds on the reflector aperture is 0.45 dB, which was not included in the results reported in Sections IV and V.

A. Impact of the Frequency Bandwidth

Fig. 18 shows the frequency behavior of the most relevant coupling coefficients of the proposed near-field QO MIMO antenna, associated with $\text{Rx}_{0,0}^{0,0}$ and $\text{Rx}_{-1,-1}^{0,0}$ array elements evaluated using GRASP. The reflector edge illumination is kept at −11 dB over the entire bandwidth. Fig. 18 shows that the co-couplings are not dispersive in frequency, and a level of signal to interference larger than 17 dB can be achieved over

the entire IEEE H-band from 250 up to 320 GHz. As the result, this antenna architecture can enable a simultaneous duplex transmission of 35 GHz bandwidth channels. When this architecture is combined with 16 wideband front ends with 16QAM[3], up to 1.2 Tbps single direction data rates can be theoretically achieved with just –35 dBm of transmitted power per antenna. The same speed could also be achieved using QPSK modulation with 16 dual-polarized front ends. Recently, several leaky wave lens antennas have been demonstrated with similar wideband performance [42]–[44] as well as low-cost manufactured horns [45], which could be potentially used in combination with a dual-reflector system to implement the proposed QO MIMO architecture.

VII. Concluding Remarks

This article presents a study of QO MIMO architecture for enabling ultrafast PtP wireless links at the 270 GHz spectral band. For this purpose, we study the use of electrically large apertures operating in the radiative near field to reach low propagation spreading losses and a high degree of spatial multiplexing capability. With the studied antenna configuration, multiple spatial and independent data streams can be transmitted and received using single element per beam focal plane arrays, facilitating the integration with active front ends at high frequencies.

A specific antenna architecture operating at 270 GHz based on a 2×2 array of parabolic reflectors combined with 2×2 focal plane arrays for a link distance of 100 m is investigated in detail. The proposed architecture is capable of transmitting 16 data streams in a 70 GHz bandwidth with signal to interference levels larger than 17 dB without the need for interference cancelation techniques. This architecture achieves higher MIMO capacity gains when compared with a classical 16×16 LoS MIMO architecture with the same level of transmitted power. Combining the proposed QO MIMO architecture with wideband front ends could potentially lead to aggregated data rates above Tbps, not previously achieved experimentally to the best of authors knowledge.

References

[1] T. S. Rappaport *et al.*, "Wireless communications and applications above 100 GHz: Opportunities and challenges for 6G and beyond," *IEEE Access*, vol. 7, pp. 78729–78757, 2019.

[2] H. Q. Ngo, E. G. Larsson, and T. L. Marzetta, "Energy and spectral efficiency of very large multiuser MIMO systems," *IEEE Trans. Commun.*, vol. 61, no. 4, pp. 1436–1449, Apr. 2013.

[3] E. Björnson, L. Sanguinetti, J. Hoydis, and M. Debbah, "Optimal design of energy-efficient multi-user MIMO systems: Is massive MIMO the answer?" *IEEE Trans. Wireless Commun.*, vol. 14, no. 6, pp. 3059–3075, Jun. 2015.

[4] T. S. Rappaport *et al.*, "Millimeter wave mobile communications for 5G cellular: It will work!" *IEEE Access*, vol. 1, pp. 335–349, 2013.

[5] IEEE Standard for High Data Rate Wireless Multi-Media Networks, *Amendment 2: 100 Gb/s Wireless Switched Point-to-Point Physical Layer*, IEEE Standard 802.15.3d-2017 (Amendment to IEEE Standard 802.15.3-2016), Oct. 2017, pp. 1–55.

[6] P. H. Siegel, "Terahertz technology," *IEEE Trans. Microw. Theory Techn.*, vol. 50, no. 3, pp. 910–928, Mar. 2002.

[7] E. G. Larsson, O. Edfors, F. Tufvesson, and T. L. Marzetta, "Massive MIMO for next generation wireless systems," *IEEE Commun. Mag.*, vol. 52, no. 2, pp. 186–195, Feb. 2014.

[8] L. Zheng and D. N. C. Tse, "Diversity and multiplexing: A fundamental tradeoff in multiple-antenna channels," *IEEE Trans. Inf. Theory*, vol. 49, no. 5, pp. 1073–1096, May 2003.

[9] Y. H. Cho and J. J. Kim, "Line-of-sight MIMO channel in millimeter-wave beamforming system: Modeling and prototype results," in *Proc. IEEE 81st Veh. Technol. Conf. (VTC)*, Glasgow, U.K., May 2015, pp. 1–5.

[10] C. Sheldon, M. Seo, E. Torkildson, M. Rodwell, and U. Madhow, "Four-channel spatial multiplexing over a millimeter-wave line-of-sight link," in *IEEE MTT-S Int. Microw. Symp. Dig.*, Boston, MA, USA, Jun. 2009, pp. 389–392.

[11] C. Sheldon, M. Seo, E. Torkildson, U. Madhow, and M. Rodwell, "A 2.4 Gb/s millimeter-wave link using adaptive spatial multiplexing," in *Proc. IEEE Antennas Propag. Soc. Int. Symp.*, Jul. 2010, pp. 1–4.

[12] X. Song *et al.*, "Design and experimental evaluation of equalization algorithms for line-of-sight spatial multiplexing at 60 GHz," *IEEE J. Sel. Areas Commun.*, vol. 36, no. 11, pp. 2570–2580, Nov. 2018.

[13] Ericsson, "Breaking the 100Gbps Barrier," Ericsson, Stockholm, Sweden, Extract Ericsson Microw. Outlook Rep. EAB-17:014270 Uen, 2019

[14] G. Gibson *et al.*, "Free-space information transfer using light beams carrying orbital angular momentum," *Opt. Exp.*, vol. 12, no. 22, pp. 5448–5456, 2004.

[15] J. Wang *et al.*, "Terabit free-space data transmission employing orbital angular momentum multiplexing," *Nature Photon.*, vol. 6, pp. 488–496, Jun. 2012.

[16] Y. Yan *et al.*, "High-capacity millimetre-wave communications with orbital angular momentum multiplexing," *Nature Commun.*, vol. 5, p. 4876, Mar. 2014.

[17] Y. Ren *et al.*, "Line-of-sight millimeter-wave communications using orbital angular momentum multiplexing combined with conventional spatial multiplexing," *IEEE Trans. Wireless Commun.*, vol. 16, no. 5, pp. 3151–3161, May 2017.

[18] O. Edfors and A. J. Johansson, "Is orbital angular momentum (OAM) based radio communication an unexploited area?" *IEEE Trans. Antennas Propag.*, vol. 60, no. 2, pp. 1126–1131, Feb. 2012.

[19] E. Björnson, J. Hoydis, M. Kountouris, and M. Debbah, "Massive MIMO systems with non-ideal hardware: Energy efficiency, estimation, and capacity limits," *IEEE Trans. Inf. Theory*, vol. 60, no. 11, pp. 7112–7139, Nov. 2014.

[20] T. Schneider, A. Wiatrek, S. Preußler, M. Grigat, and R.-P. Braun, "Link budget analysis for terahertz fixed wireless links," *IEEE Trans. THz Sci. Technol.*, vol. 2, no. 2, pp. 250–256, Mar. 2012.

[21] G. V. Borgiotti, "Maximum power transfer between two planar apertures in the Fresnel zone," *IEEE Trans. Antennas Propag.*, vol. AP-14, no. 2, pp. 158–163, Mar. 1966.

[22] J. D. Heebl, M. Ettorre, and A. Grbic, "Wireless links in the radiative near field via Bessel beams," *Phys. Rev. Appl.*, vol. 6, no. 3, 2016, Art. no. 034018.

[23] V. R. Gowda, O. Yurduseven, G. Lipworth, T. Zupan, M. S. Reynolds, and D. R. Smith, "Wireless power transfer in the radiative near field," *IEEE Antennas Wireless Propag. Lett.*, vol. 15, pp. 1865–1868, 2016.

[24] V. Rumsey, "On the design and performance of feeds for correcting spherical aberration," *IEEE Trans. Antennas Propag.*, vol. AP-18, no. 3, pp. 343–351, May 1970.

[25] M. A. Campo, D. Blanco, S. Bruni, A. Neto, and N. Llombart, "On the use of Fly's eye lenses with leaky-wave feeds for wideband communications," *IEEE Trans. Antennas Propag.*, vol. 68, no. 4, pp. 2480–2493, Apr. 2020.

[26] S. Carpenter *et al.*, "A-band 48-Gbit/s 64-QAM/QPSK direct-conversion I/Q transceiver chipset," *IEEE Trans. Microw. Theory Techn.*, vol. 64, no. 4, pp. 1285–1296, Apr. 2016.

[27] P. Rodriguez-Vazquez, J. Grzyb, B. Heinemann, and U. R. Pfeiffer, "A 16-QAM 100-Gb/s 1-M wireless link with an EVM of 17% at 230 GHz in an SiGe technology," *IEEE Microw. Wireless Compon. Lett.*, vol. 29, no. 4, pp. 297–299, Apr. 2019.

[28] I. Kallfass *et al.*, "64 Gbit/s transmission over 850 m fixed wireless link at 240 GHz carrier frequency," *J. Infr., Millim., THz Waves*, vol. 36, no. 2, pp. 221–233, Feb. 2015.

[29] I. Dan *et al.*, "A 300-GHz wireless link employing a photonic transmitter and an active electronic receiver with a transmission bandwidth of 54 GHz," *IEEE Trans. THz Sci. Technol.*, vol. 10, no. 3, pp. 271–281, May 2020.

[3]0.2 roll-off is assumed.

[30] E. Telatar, "Capacity of multi-antenna Gaussian channels," *Eur. Trans. Telecommun.*, vol. 10, no. 6, pp. 585–595, 1999.
[31] J. Brady, N. Behdad, and A. M. Sayeed, "Beamspace MIMO for millimeter-wave communications: System architecture, modeling, analysis, and measurements," *IEEE Trans. Antennas Propag.*, vol. 61, no. 7, pp. 3814–3827, Jul. 2013.
[32] C. Sheldon, E. Torkildson, M. Seo, C. P. Yue, U. Madhow, and M. Rodwell, "A 60 GHz line-of-sight 2x2 MIMO link operating at 1.2 Gbps," in *Proc. IEEE Antennas Propag. Soc. Int. Symp.*, Jul. 2008, pp. 1–4.
[33] Y. Xue, X. Zheng, and V. K. N. Lau, "Line-of-sight MIMO for high capacity millimeter wave backhaul in FDD systems," *J. Commun. Inf. Netw.*, vol. 5, no. 2, pp. 177–193, Jun. 2020.
[34] R. C. Hansen, "Aperture theory," in *Microwave Scanning Antennas: Apertures*. New York, NY, USA: Academic, 1964.
[35] S. M. Mikki, S. Clauzier, and Y. M. M. Antar, "Empirical geometrical bounds on MIMO antenna arrays for optimum diversity gain performance: An electromagnetic design approach," *IEEE Access*, vol. 6, pp. 39876–39894, 2018.
[36] J. Proakis and M. Salehi, *Digital Communications*. New York, NY, USA: McGraw-Hill, 2007.
[37] K. B. Cooper, R. J. Dengler, N. Llombart, B. Thomas, G. Chattopadhyay, and P. H. Siegel, "THz imaging radar for standoff personnel screening," *IEEE Trans. THz Sci. Technol.*, vol. 1, no. 1, pp. 169–182, Sep. 2011.
[38] D. A. Robertson *et al.*, "The CONSORTIS 16-channel 340-GHz security imaging radar," in *Proc. SPIE, 21st Passive Act. Millim.-Wave Imag.*, 2018, Art. no. 1063409.
[39] S. K. Rao, "Design and analysis of multiple-beam reflector antennas," *IEEE Antennas Propag. Mag.*, vol. 41, no. 4, pp. 53–59, Aug. 1999.
[40] S. O. Dabironezare, G. Carluccio, A. Neto, and N. Llombart, "Wide band wide scan quasi-optical systems: A Fourier optics-geometrical optics based analysis," in *Proc. IEEE Int. Symp. Antennas Propag. (APS)*, Dec. 2021.
[41] *TICRA Tools Software*, GRASP Version 19.1.1, Copenhagen, Denmark, 2019.
[42] M. A. Campo, G. Carluccio, D. Blanco, O. Litschke, S. Bruni, and N. Llombart, "Wideband circularly polarized antenna with in-lens polarizer for high-speed communications," *IEEE Trans. Antennas Propag.*, vol. 69, no. 1, pp. 43–54, Jan. 2021.
[43] M. A. Campo *et al.*, "H-band quartz-silicon leaky-wave lens with air-bridge interconnect to GaAs front-end," *IEEE Trans. THz Sci. Technol.*, vol. 11, no. 3, pp. 297–309, May 2021.
[44] O. Yurduseven, N. L. Juan, and A. Neto, "A dual-polarized leaky lens antenna for wideband focal plane arrays," *IEEE Trans. Antennas Propag.*, vol. 64, no. 8, pp. 3330–3337, Aug. 2016.
[45] B. Aqlan, M. Himdi, L. L. Coq, and H. Vettikalladi, "Sub-THz circularly polarized horn antenna using wire electrical discharge machining for 6G wireless communications," *IEEE Access*, vol. 8, pp. 117245–117252, 2020.

Nuria Llombart (Fellow, IEEE) received the master's degree in electrical engineering and the Ph.D. degree from the Polytechnic University of Valencia, Valencia, Spain, in 2002 and 2006, respectively.

During her master's degree studies, she spent one year at the Friedrich-Alexander University of Erlangen-Nuremberg, Erlangen, Germany, and was with the Fraunhofer Institute for Integrated Circuits, Erlangen. From 2002 to 2007, she was with the Antenna Group, TNO Defense, Security and Safety Institute, The Hague, The Netherlands, where she is currently a Ph.D. Student and afterward as a Researcher. From 2007 to 2010, she was a Post-Doctoral Fellow with the California Institute of Technology, Pasadena, CA, USA. She is currently with the Submillimeter Wave Advance Technology Group, Jet Propulsion Laboratory, Pasadena, CA. She was a "Ramón y Cajal" Fellow with the Optics Department, Complutense University of Madrid, Madrid, Spain, from 2010 to 2012. In 2012, she joined the THz Sensing Group, Technical University of Delft, Delft, The Netherlands, where she joined as a Full Professor in 2018. She has coauthored more than 150 journal and international conference contributions. Her research interests include the analysis and design of planar antennas, periodic structures, reflector antennas, lens antennas, and waveguide structures, with an emphasis on the terahertz range.

Dr. Llombart serves as a Board Member for the IRMMW-THz International Society. She was a recipient of the H. A. Wheeler Award for the Best Applications Paper of 2008 in the IEEE TRANSACTIONS ON ANTENNAS AND PROPAGATION, the 2014 THz Science and Technology Best Paper Award of the IEEE Microwave Theory and Techniques Society, several NASA awards, the 2014 IEEE Antenna and Propagation Society Lot Shafai Mid-Career Distinguished Achievement Award, and the European Research Council Starting Grant in 2015.

Shahab Oddin Dabironezare (Member, IEEE) was born in Mashhad, Iran. He received the M.Sc. and Ph.D. degrees in electrical engineering from Delft University of Technology, Delft, The Netherlands, in 2015 and 2020, respectively.

He is currently a Post-Doctoral Researcher with the Microelectronics Department, THz Sensing Group, Delft University of Technology. His research interests include wideband antennas at millimeter and submillimeter-wave applications, wide field-of-view imaging systems, quasi-optical systems, lens antennas, and absorber-based passive cameras.